S1. Errors in GEOS-5 meteorological parameters

Errors in the GEOS-5 meteorology are quantified here using observational data from ISH and ISCCP. Results are exploited in Sect. 4 to evaluate the sensitivity of NO_2 columns simulated by GEOS-Chem to meteorological inputs.

To better understand the reliability of the meteorological fields, the analysis is conducted for a comprehensive set of parameters including air temperature, RH, tropospheric water vapor path, surface air pressure, 10m wind speed, cloud fraction, COD, and precipitation. Measurements are taken from the ISH dataset for air temperature, RH, surface air pressure, wind speed and precipitation, and are taken from ISCCP for tropospheric water vapor path, cloud fraction and COD. The analysis is emphasized in the daytime, particularly at mid-day when the lifetime of NOx is shortest and has the largest impact on its abundance at the overpass time of OMI (i.e., in the early afternoon).

S1.1 Air temperature

Surface (2m) air temperature in GEOS-5 differs from the NCDC ISH data (Fig. S1). In July, the GEOS-5 temperature at mid-day (mean over 0300-0600 UTC, or 11:00-14:00 Beijing local time (BLT)) is weakly correlated to the ISH data spatially, with an R^2 of 0.27. It is higher than ISH by 5 ℃ or more in parts of the north but lower than ISH by 0-2 ℃ in most of the south (Fig. S1). Averaged over East China, there exist positive biases in the daytime and negative biases at night (Fig. S1). For January, the spatial correlation between the two datasets increases significantly for mid-day temperature: the R^2 reaches 0.95. This is due mainly to the enhanced latitudinal temperature gradient from summer to winter captured by GEOS-5. Averaged over East China, GEOS-5 overestimates the ISH temperature by about 0.9 – 2.3 ℃ during the daytime and slightly underestimates it at night (Fig. S1). The temperature biases are caused in part by errors in cloud amount and COD (see Sect. S1.6) affecting the amount of radiation reaching the ground.

S1.2 Relative humidity

At mid-day, RH in the surface air (2m) also differs between GEOS-5 and ISH as a result of differences in air temperature and water vapor (Fig. S2). In July, the GEOS-5 RH is about 10-30% lower than ISH in the north but 10-20% higher in the south (Fig. S2). It is lower than ISH at most stations in January (Fig. S2). The spatial correlation between GEOS-5 and ISH differs from that for air temperature: the R^2 increases to 0.48 in July and decreases to 0.39 for January. Diurnally, the GEOS-5 RH is lower than ISH during the daytime but is higher than ISH at night averaged over East China (Fig. S2).

S1.3 Tropospheric water vapor path

Measurements of water vapor path are taken from ISCCP with no information for diurnal variation. For daily mean values in July, the GEOS-5 dataset underestimates the water vapor path in ISCCP by more than 10% in most of the north, northwest, and southwest where the ISCCP values are normally lower than 5 cm (Fig. S3). It overestimates the ISCCP measurements in other regions with the ISCCP values exceeding 5 cm (Fig. S3). The R^2 for spatial correlation is about 0.59. Water vapor path decreases significantly from July to January, when the spatial variability in ISCCP is better captured by GEOS-5 resulting in a large R^2 of 0.78. In January, however, GEOS-5 underestimates the ISCCP water vapor path at most stations (Fig. S3).

S1.4 Surface air pressure

Day-to-day variation in surface air pressure is a good indicator of the large-scale circulation propagating through different regions of East China. The observed variation in ISH is reproduced by GEOS-5 with the R^2 close to unity in both January and July (Fig. S4), suggesting that the large-scale circulation is well constrained by the assimilation system. Meanwhile, the GEOS-5 data are in general lower than ISH with an average bias of about 10 hPa for East China in both months (Fig. S4). The bias decreases to 1 hPa or less averaged over Northern East China (111.5°-122°E, 29°-41°N; Fig. S4), the main polluted region of China with a flatter terrain.

S1.5 Wind speed at 10m

Daily mean wind speed at 10m in GEOS-5 is normally much larger than ISH for both January and July, especially over regions of low wind speed (Fig. S5). Averaged over East China, the GEOS-5 wind speed is about 3.5 m/s in both months whereas the ISH winds are only about 2.4 – 2.5 m/s. The R^2 is 0.35 – 0.37 in the two months for spatial correlation between GEOS-5 and ISH. The correlation is high between the two datasets for diurnal variation, with the R^2 reaching 0.74 – 0.78 in the two months.

S1.6 Cloud fraction and COD

The mid-day cloud fraction in GEOS-5 differs significantly from the ISCCP data (Fig. S6). In July, the GEOS-5 cloud fraction is lower than ISCCP by about 0.25 over most of East China but is slightly higher than ISCCP over the southern coastal regions. In January, GEOS-5 is about 0.1 – 0.25 lower than ISCCP in the north and the negative bias exceeds 0.5 in parts of the southern provinces. The correlation is low between the two datasets for both spatial and diurnal variations.

To evaluate the GEOS-5 COD, the in-cloud COD in ISCCP is converted to radiative mean COD taking into account the amount of cloud fraction (Liu et al., 2009). Correspondingly, the radiative mean COD for GEOS-5 is calculated as the sum over all tropospheric layers of the product of in-cloud COD and cloud fraction raised to the 1.5th power assuming an approximate random overlap of clouds vertically (Liu et al., 2009). As with cloud fraction, the mid-day radiative mean COD derived from GEOS-5 differs significantly from that based on ISCCP (Fig. S7). In July, the GEOS-5 COD is lower than ISCCP by 0.5 – 3 in most areas. In January, the negative biases exceed 5 in parts of the south and are less than 1 in the north. The relative (percentage) error exceeds 50% in most areas for both months. Spatially and diurnally, the correlation is low between the two datasets. The relative errors for daytime mean COD in GEOS-5 are similar to those at mid-day (not shown).

S1.7 Precipitation

On the regional mean basis, the amount of daily precipitation in GEOS-5 is consistent with ISH. In GEOS-5, daily precipitation exhibits significant seasonal variability, with a regional mean of 6.3 mm/day in July and 0.95 mm/day in January. Meanwhile, the regional mean for ISH is about 5.7 mm/day in July and 0.77 mm/day in January. Differences between GEOS-5 and ISH are larger at individual stations (Fig. S8). The R^2 is 0.42 – 0.43 in the two months for spatial correlation between the two datasets.

S2. PBLH provided by GEOS-5

The GEOS-5 PBLH is diagnosed as the height of the lowest layer in which the eddy diffusivity is smaller than 2 $m^2\ s^{-1}$ (Global Modeling and Assimilation Office, 2006). Across East China, its values in the afternoon (13:00-15:00 Beijing local time; around the overpass time of OMI) exhibit significant seasonal variation due to changes in static and mechanic instability. In July, the afternoon height exceeds 2000m over the arid/semiarid northwest but is only about 1000m in the coastal provinces in the east and south (Fig. S11). In January, it reaches 2000m in parts of the west but is as low as about 750m in the north (Fig. S11). At night, the PBLH in GEOS-5 is less than 100m in most days of the two months over China and other continental areas (not shown).

Overall, the GEOS-5 PBLH may be overestimated in the daytime due to positive biases in surface air temperature enhancing the static instability; while it may be underestimated at night as a result of negative temperature biases. The observation-based analysis for the U.S. by Liu and Liang (2010) suggested the nighttime PBLH to be about 200-300m in all seasons, about 3 times as large as the GEOS-5 values. The magnitude of nighttime errors is adopted for China in lack of observations for independent evaluation.

S3. Chemical mechanisms not evaluated quantitatively in this study

Li et al. (2008; 2009) suggested a reaction of NO_2, excited by solar radiation > 420 nm, with water vapor to produce OH and nitrous acid (HONO). The reaction was estimated to be important at high solar zenith angles with low OH content, i.e., at twilight and/or at high latitudes. However, Carr et al. (2009) suggested a much smaller rate constant and thus negligible impacts on the tropospheric chemistry. The contradiction does not allow for conclusive determination of the true importance of the reaction (Sander et al., 2011).

A recent study by Su et al. (2011) suggested a significant source of HONO from soil nitrites, particularly from fertilized soils at low pH values. The subsequent photolysis of HONO leads to production of NO and OH, enhancing both source and sink of NOx likely with a small net impact on its abundance in the troposphere.

Karl et al. (2010) suggested dry deposition of oxygenated VOC to be much larger than normally assumed over deciduous ecosystems. They suggested a consequent enhancement of OH by 0-4% with a reduction of ozone by 1-3.5% over East China above the continental surface layer in September. The resulting impacts on model NO_2 columns are expected to be relatively small on the regional scale.

S4. Considerations for parameters not accounted for in the post-model modification

Potential errors in modeled PBL mixing are not accounted for here in lack of adequate measurements; the likely underestimate in the nighttime PBLH only has a small impact on modeled NO_2 columns in the afternoon (Fig. 6c,d; see Sect. 4.4). Potential yield of HNO_3

from reaction of NO and HO_2 needs to be confirmed by more lab experiments. Errors in emissions of CO and SO_2 are also not taken into account due to lack of adequate information (Fortems-Cheiney et al., 2011; Lu et al., 2011). Errors in NOx emissions may affect modeling of the non-linear photochemistry (see Sect. 5.6); they are however not accounted for in this section aiming to evaluate the model performance with a given amount of NOx emissions.

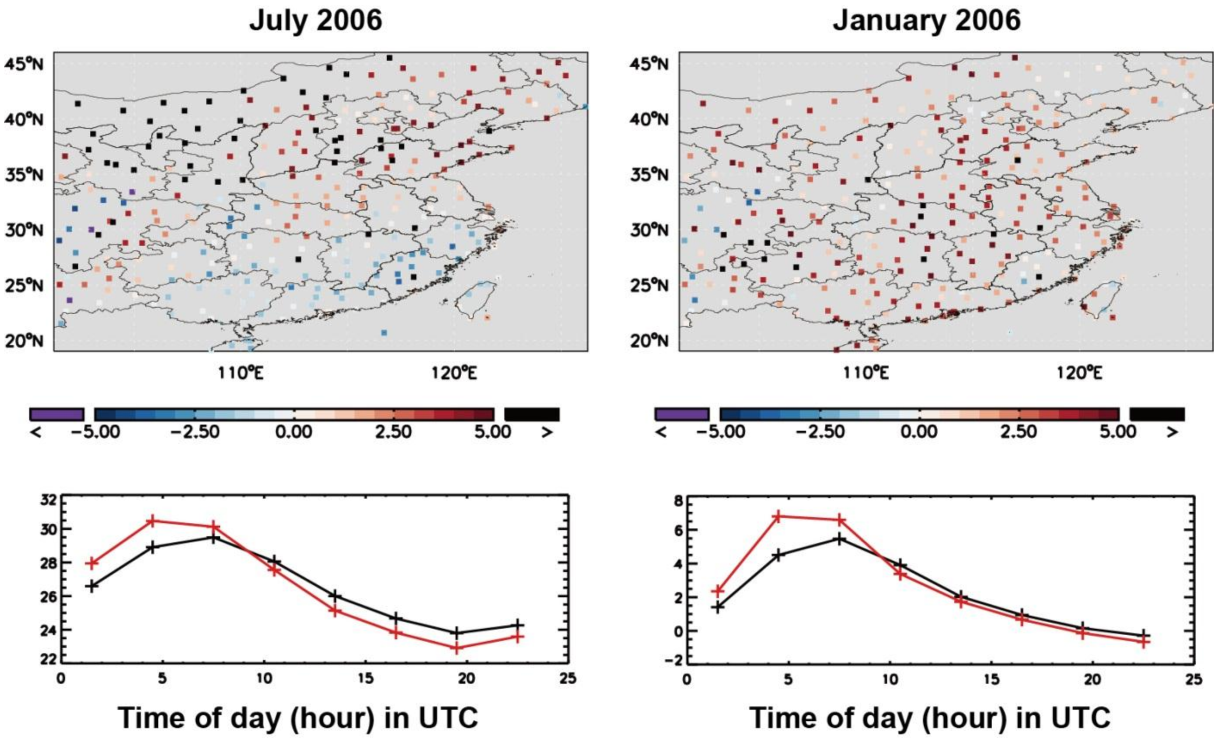

Fig. S1. (top) Differences (℃) between GEOS-5 and ISH in monthly mean near-surface air temperature at mid-day (11:00-14:00 BLT). (bottom) Diurnal variation of air temperature (℃) in ISH (black) and GEOS-5 (red) averaged over East China. Data are presented at three-hour intervals (0000-0300 UTC mean, 0300-0600 UTC mean, etc.).

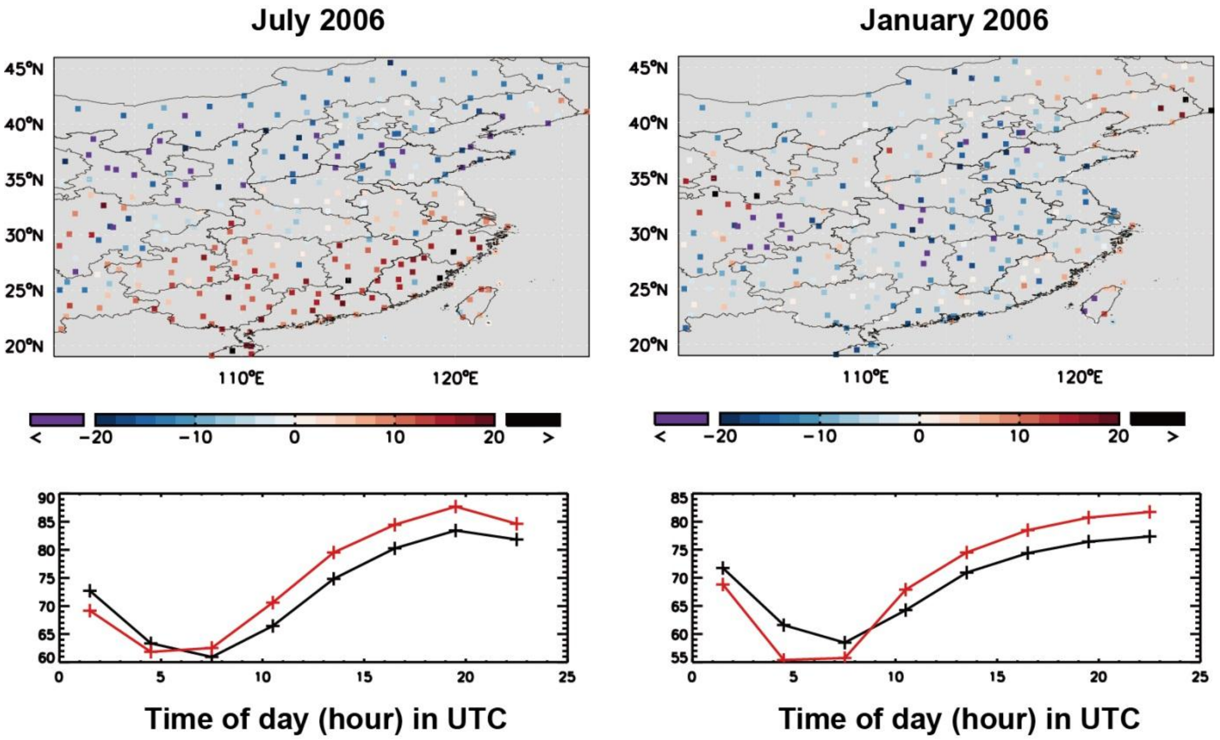

Fig. S2. Similar to Fig. S1 but for near-surface relative humidity (%).

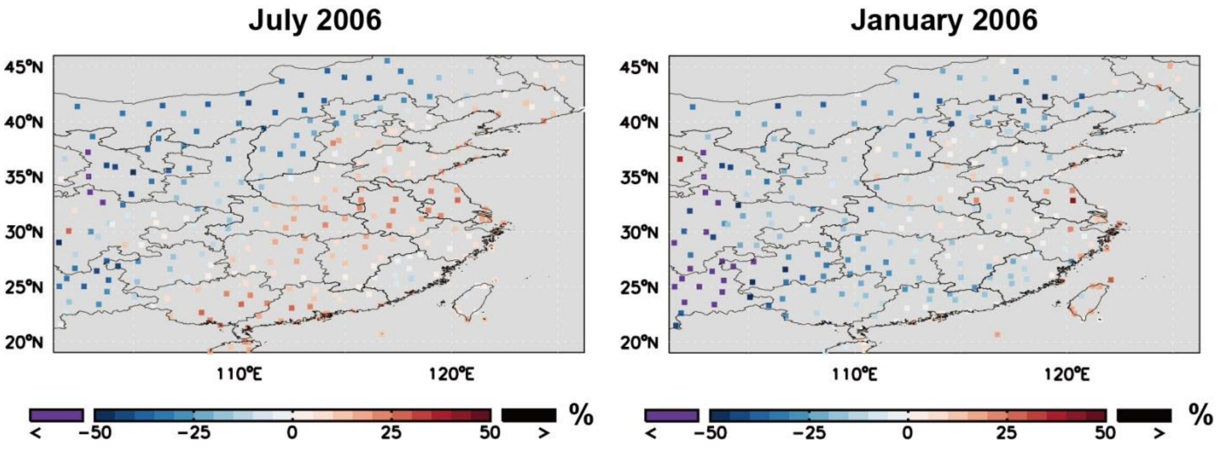

Fig. S3. (top) Percentage differences between GEOS-5 and ISCCP in monthly mean daily mean tropospheric water vapor path.

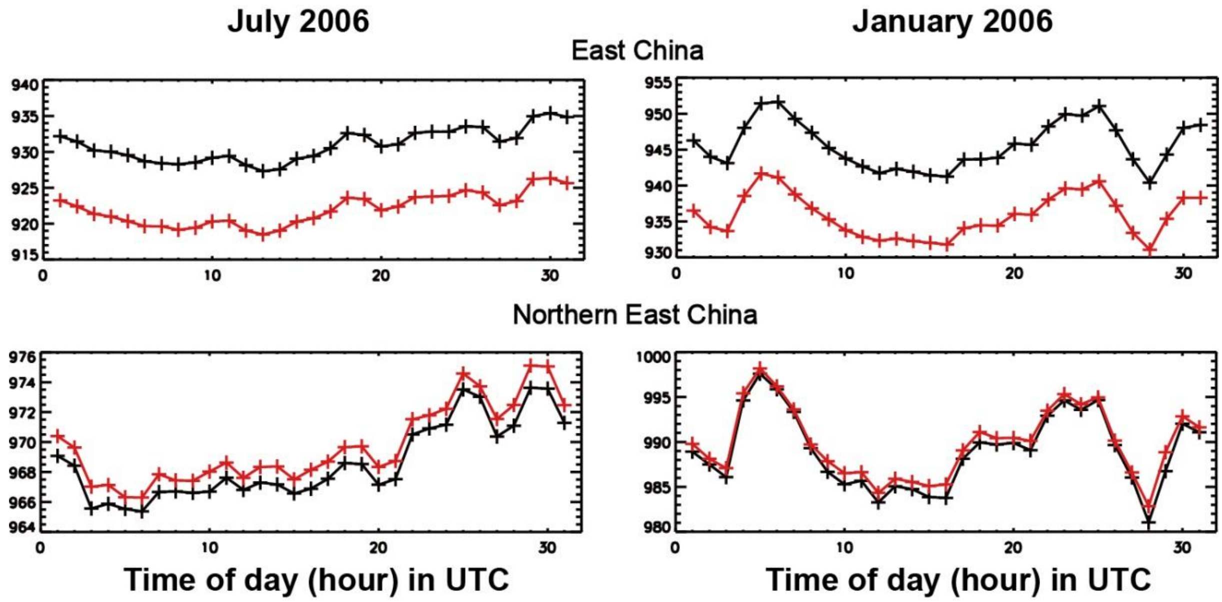

Fig. S4. Daily variation of surface air pressure in ISH (black) and GEOS-5 (red). Northern East China covers 111.5°-122°E and 29°-41°N.

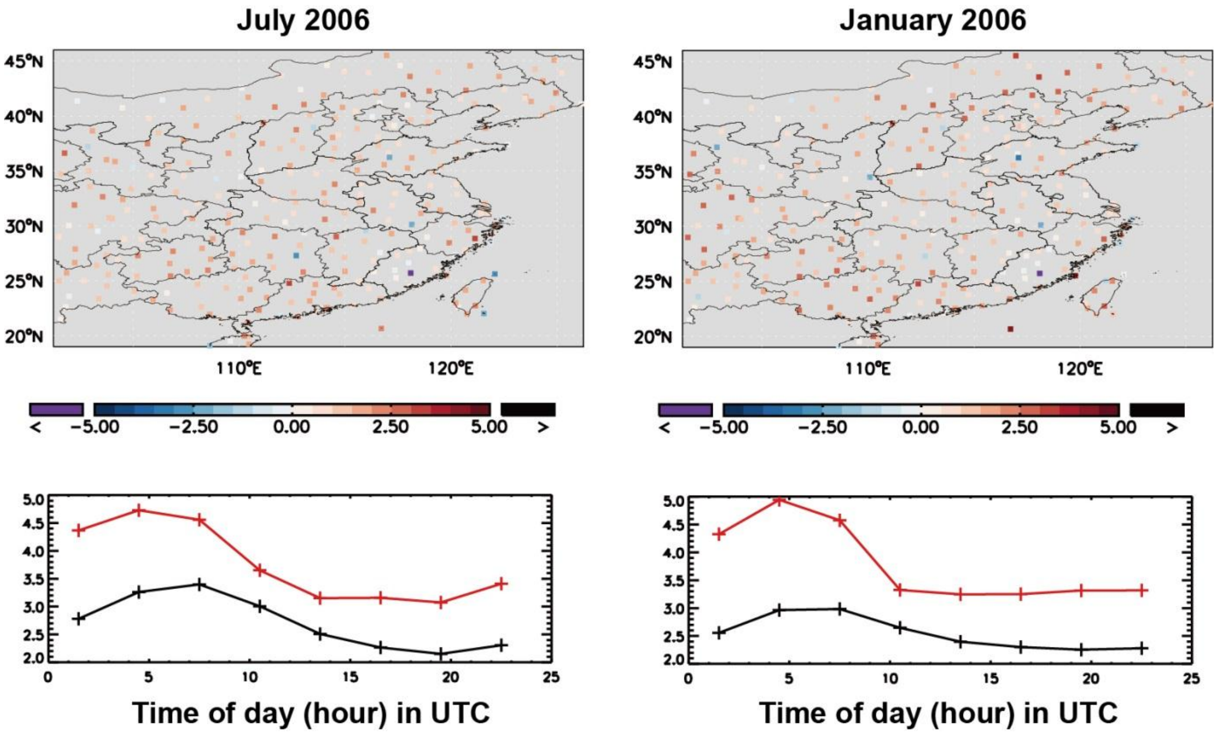

Fig. S5. (top) Differences (m s^{-1}) between GEOS-5 and ISH in monthly mean daily mean 10m wind speed. (bottom) Diurnal variation of wind speed (m s^{-1}) in ISH (black) and GEOS-5 (red) averaged over East China. Data are presented at three-hour intervals (0000-0300 UTC mean, 0300-0600 UTC mean, etc.).

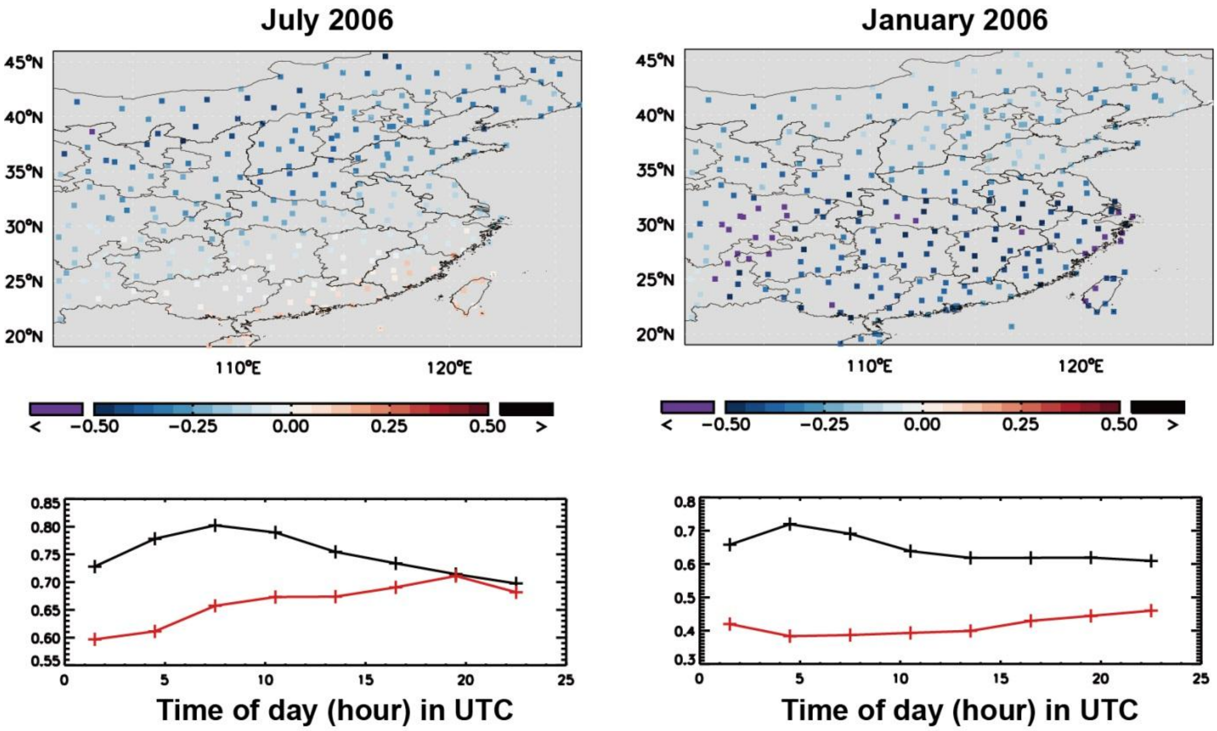

Fig. S6. Similar to Fig. S1 but for comparison of cloud fraction between GEOS-5 and ISCCP.

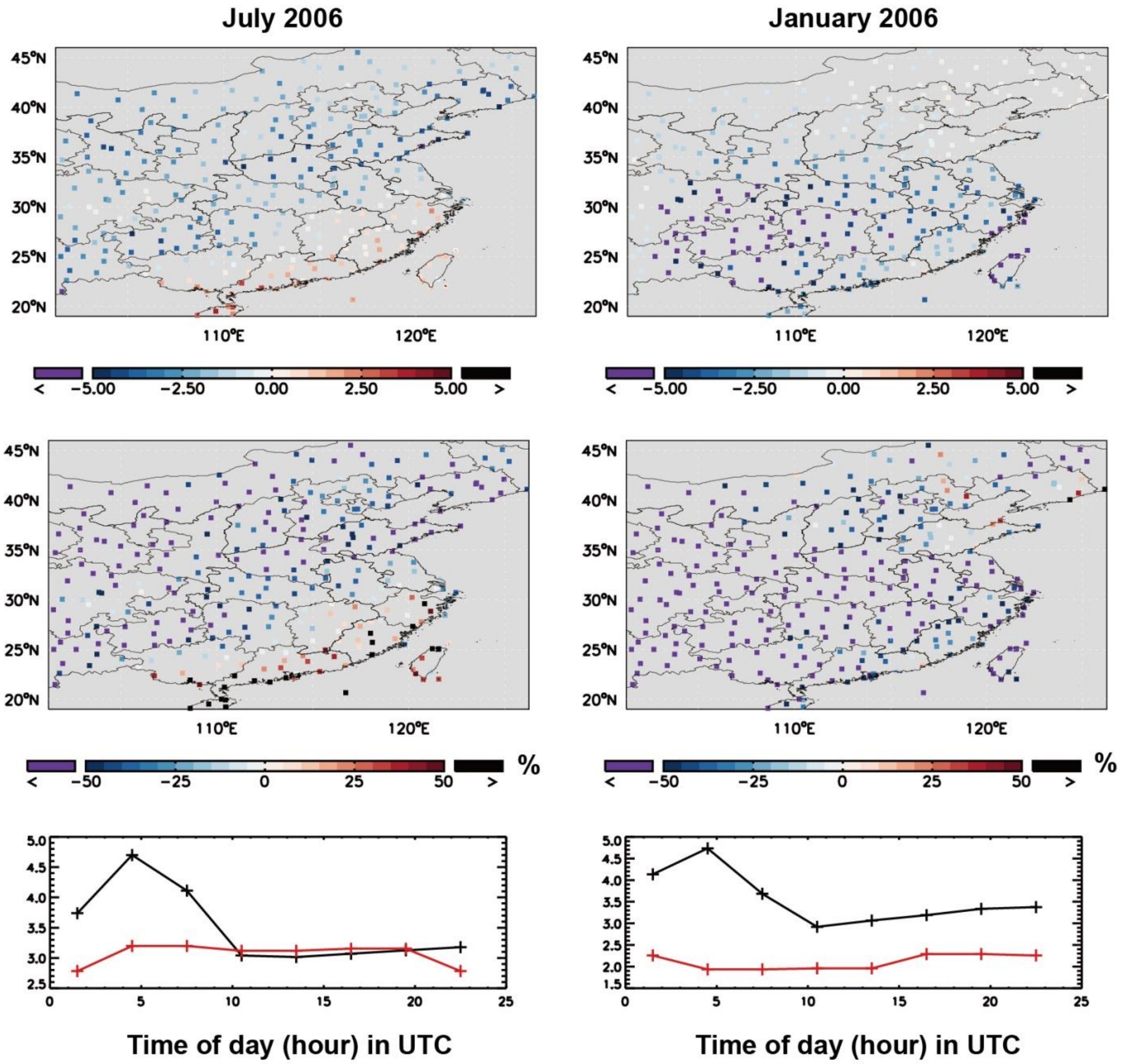

Fig. S7. (top) Differences between GEOS-5 and ISCCP in monthly mean radiative mean cloud optical depth at mid-day (11:00-14:00 BLT). (middle) The respective percentage differences. (bottom) Diurnal variation of radiative mean cloud optical depth in ISCCP (black) and GEOS-5 (red) averaged over East China. Data are presented at three-hour intervals (0000-0300 UTC mean, 0300-0600 UTC mean, etc.).

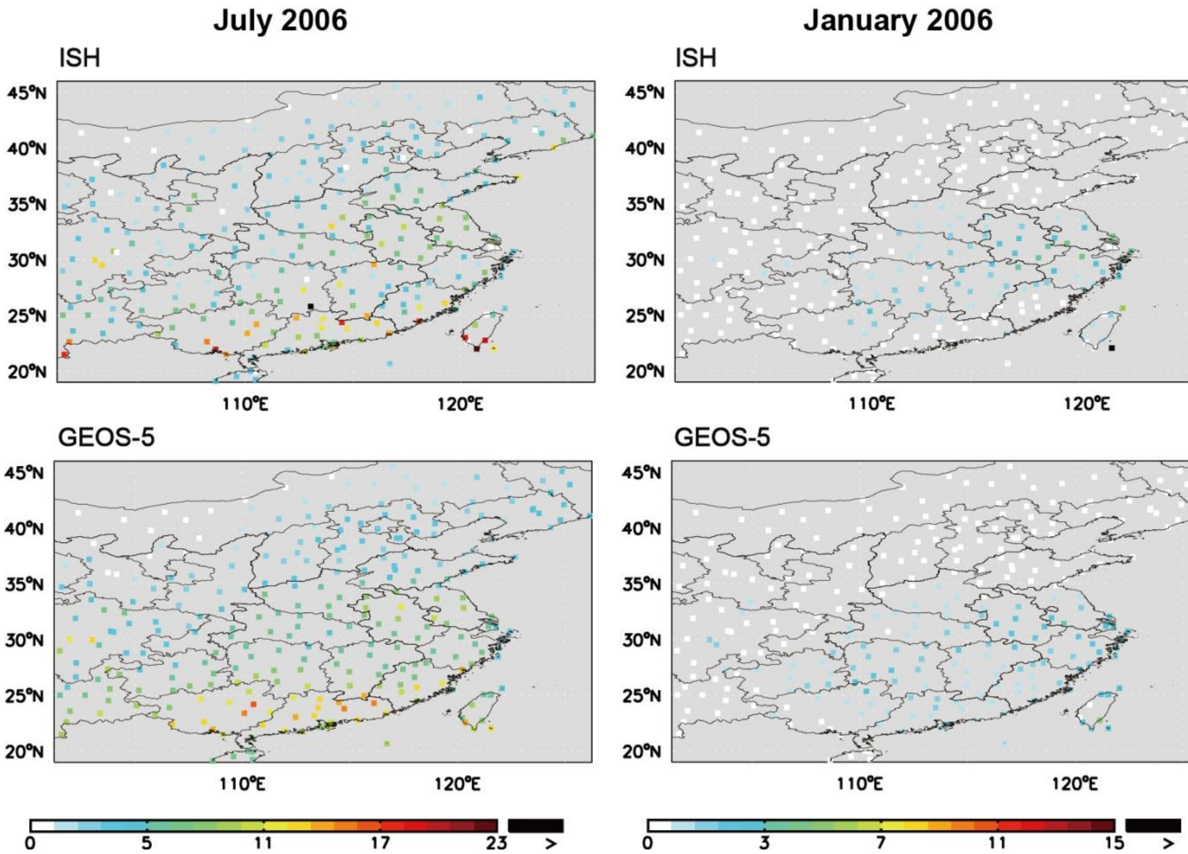

Fig. S8. Spatial distribution of monthly mean daily precipitation (mm d^{-1}) in ISH and GEOS-5.

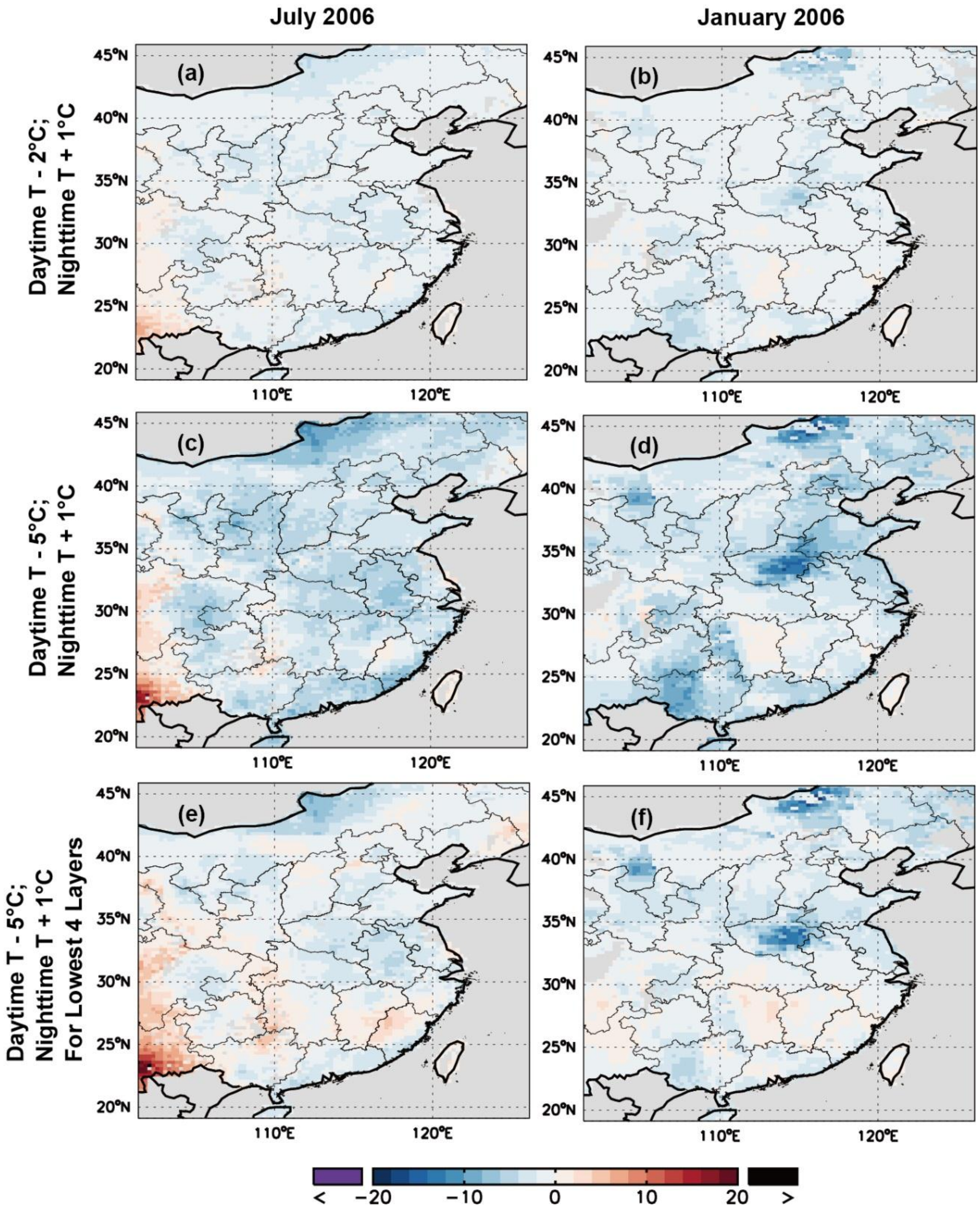

Fig. S9. Spatial distribution of percentage differences between modeled NO_2 columns with and without adjustments in air temperature. (a,b) The daytime temperature is decreased by 2 ℃ with an increase of 1 ℃ at night for the lowest 10 model layers. (c,d) The daytime temperature is decreased by 5 ℃ with an increase of 1 ℃ at night for the lowest 10 model layers. (e,f) The daytime temperature is decreased by 5 ℃ with an increase of 1 ℃ at night for the lowest four model layers. Panels (c,d) are the same as Fig. 3.

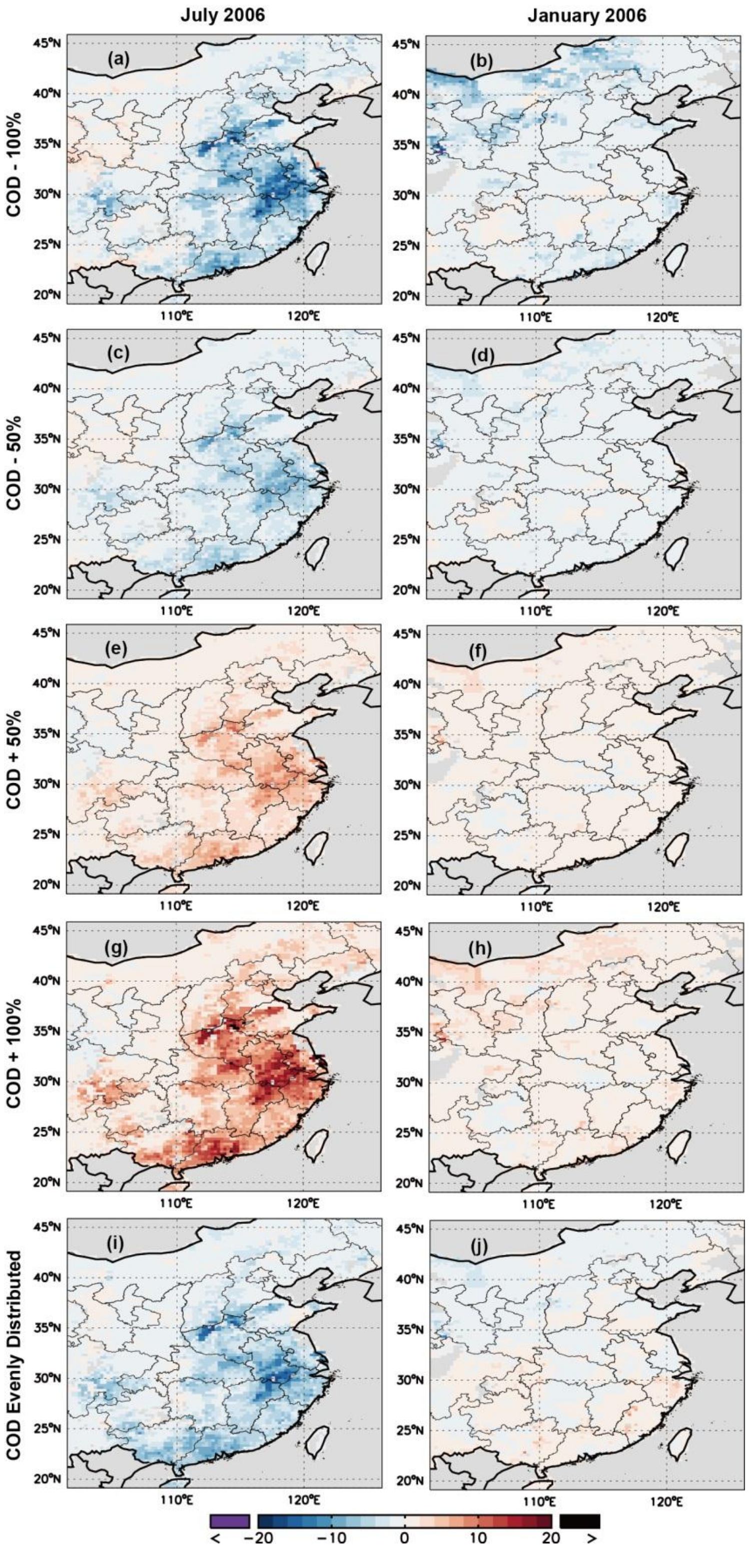

Fig. S10. Spatial distribution of percentage differences between modeled NO_2 columns with and without adjustments in COD. The COD is scaled by a factor of 0% (a,b), 50% (c,d), 150% (e,f) and 200% (g,h); or is assumed to be distributed evenly in all tropospheric layers (i,j). Panels (g,h) are the same as Fig. 5.

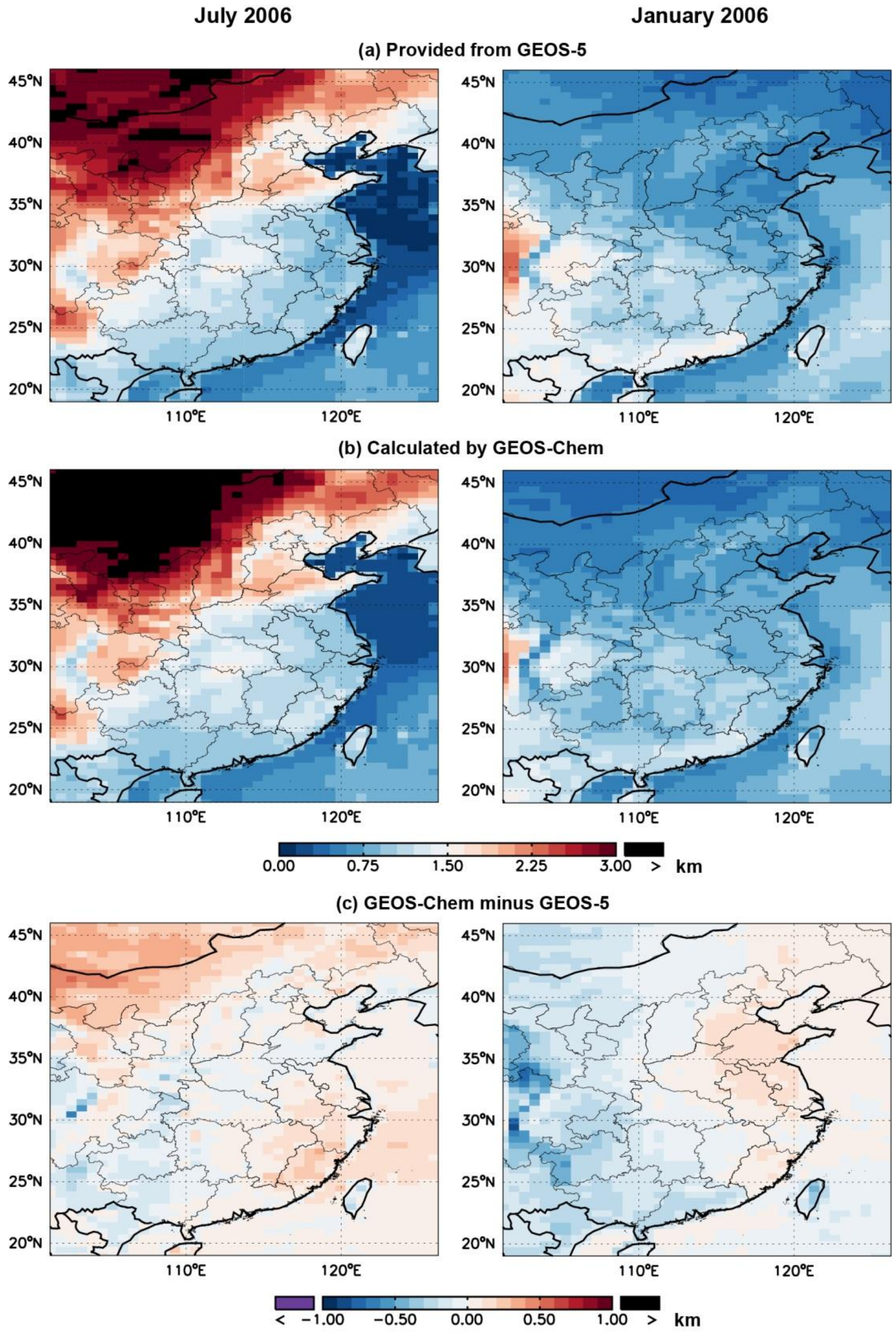

Fig. S11. PBLH taken from GEOS-5 versus PBLH calculated by GEOS-Chem at 13:00-15:00 local time (i.e., around the overpass time of OMI).

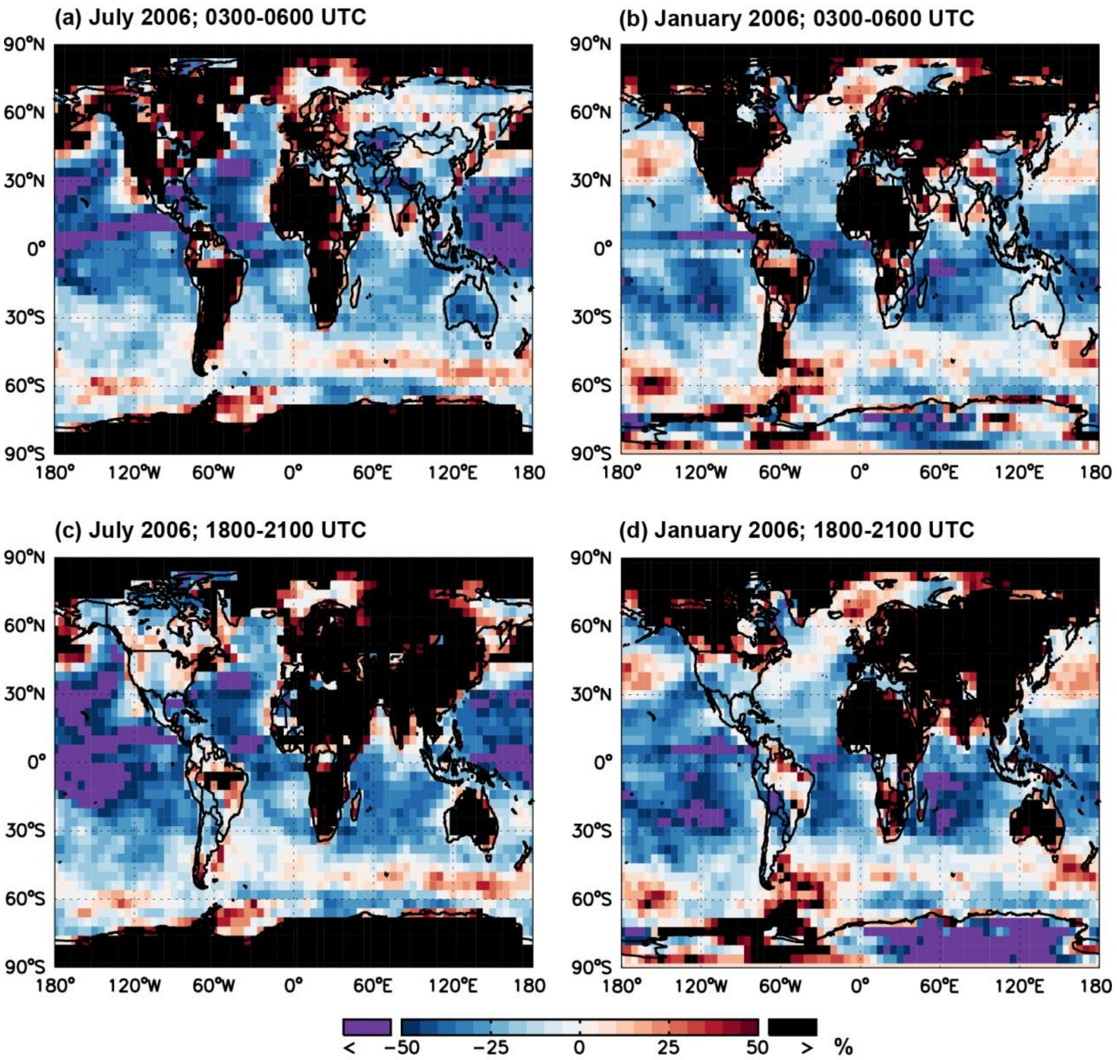

Fig. S12. Percentage differences of the GEOS-4 PBLH relative to GEOS-5 on the 2.5 ° long x 2 ° lat grid. The local time is around mid-day in Beijing and before mid-night in New York in (a,b); and is after mid-night in Beijing and in the early afternoon in New York in (c,d).

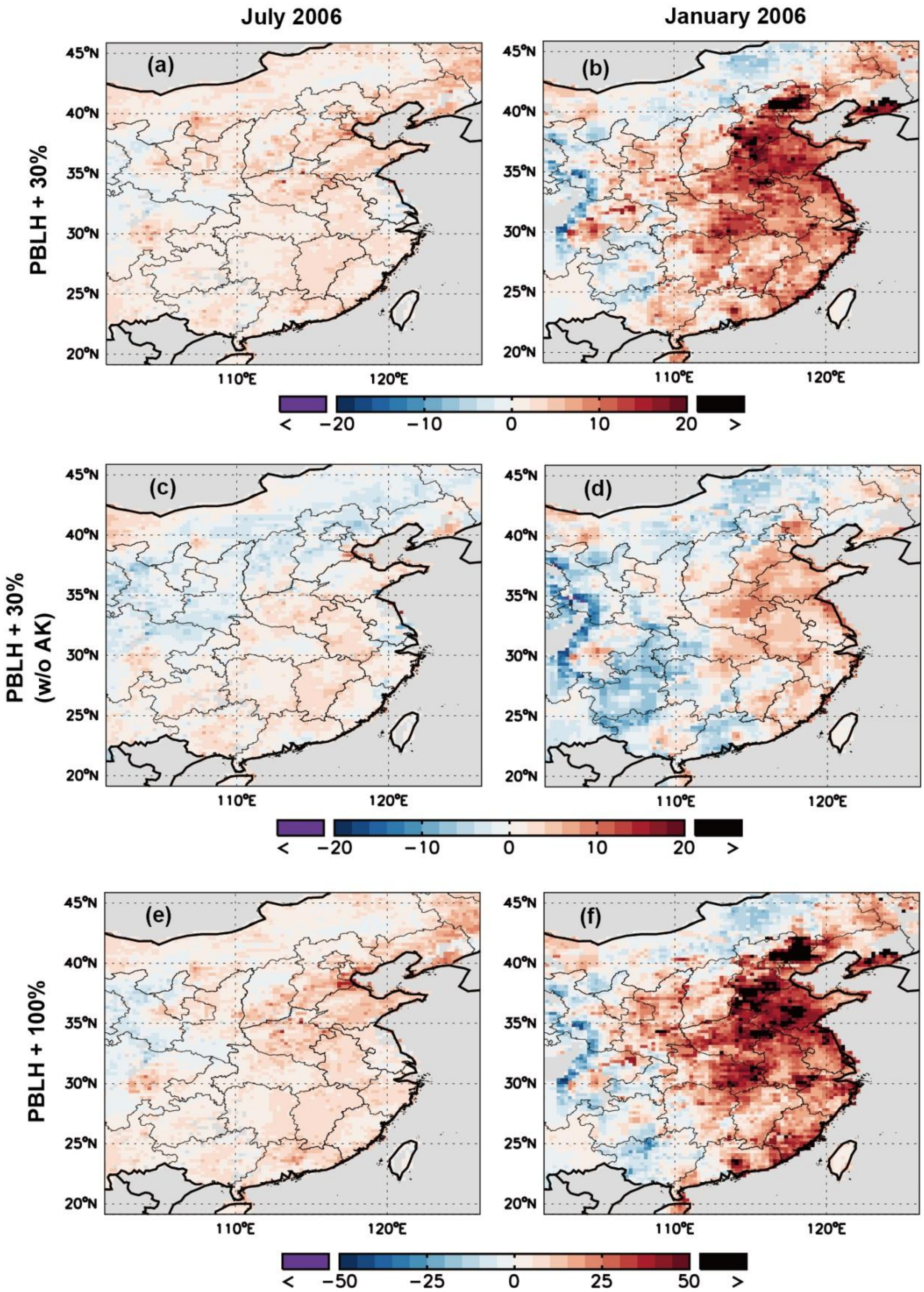

Fig. S13. Spatial distribution of percentage differences between modeled NO_2 columns with and without adjustments in PBLH. (a,b) The PBLH is increased by 30%. (c,d) The same as (a,b) but model results are not applied with AK. (e,f) The PBLH is increased by 100%.

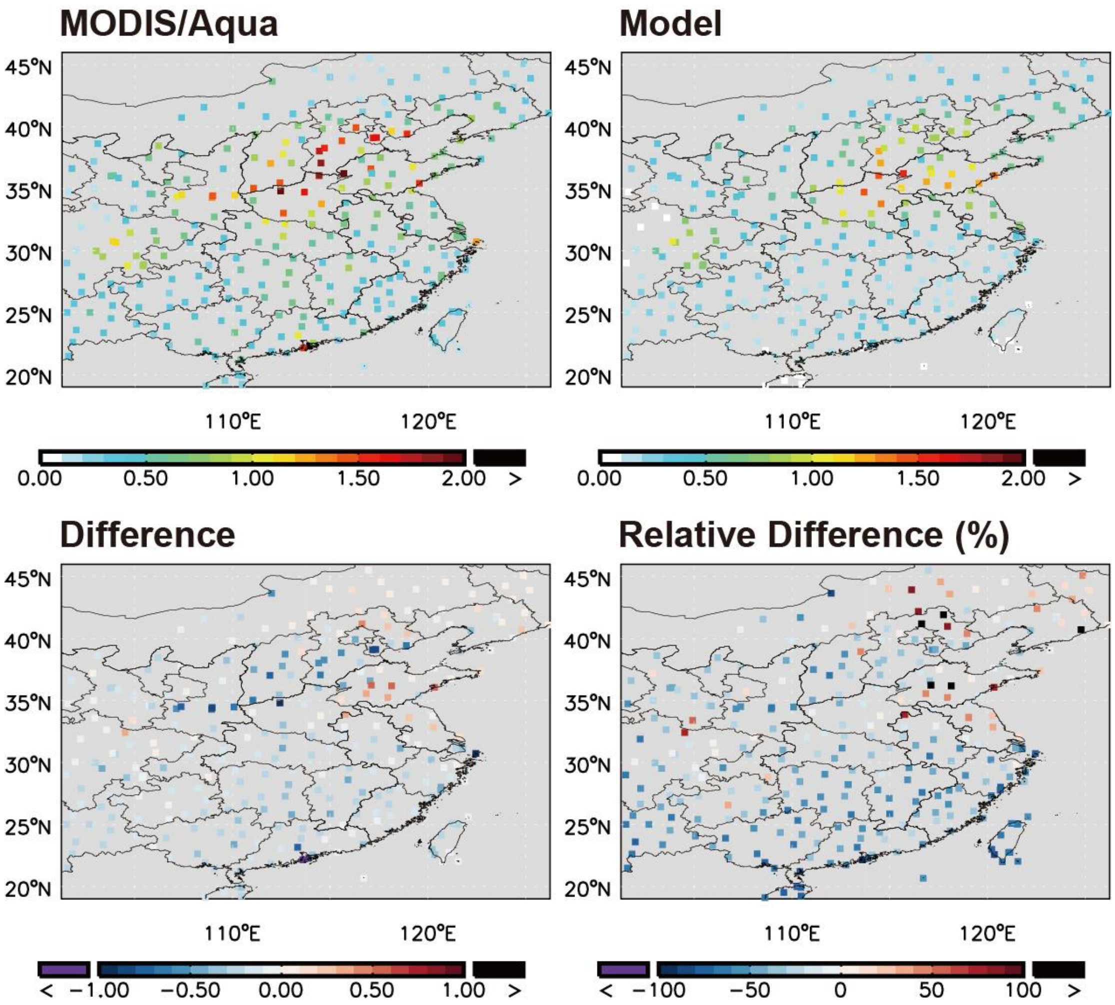

Fig. S14. July mean AOD in MODIS versus GEOS-Chem. Model values are sampled at 13:00-15:00 local time in days with valid MODIS data for a consistent comparison.

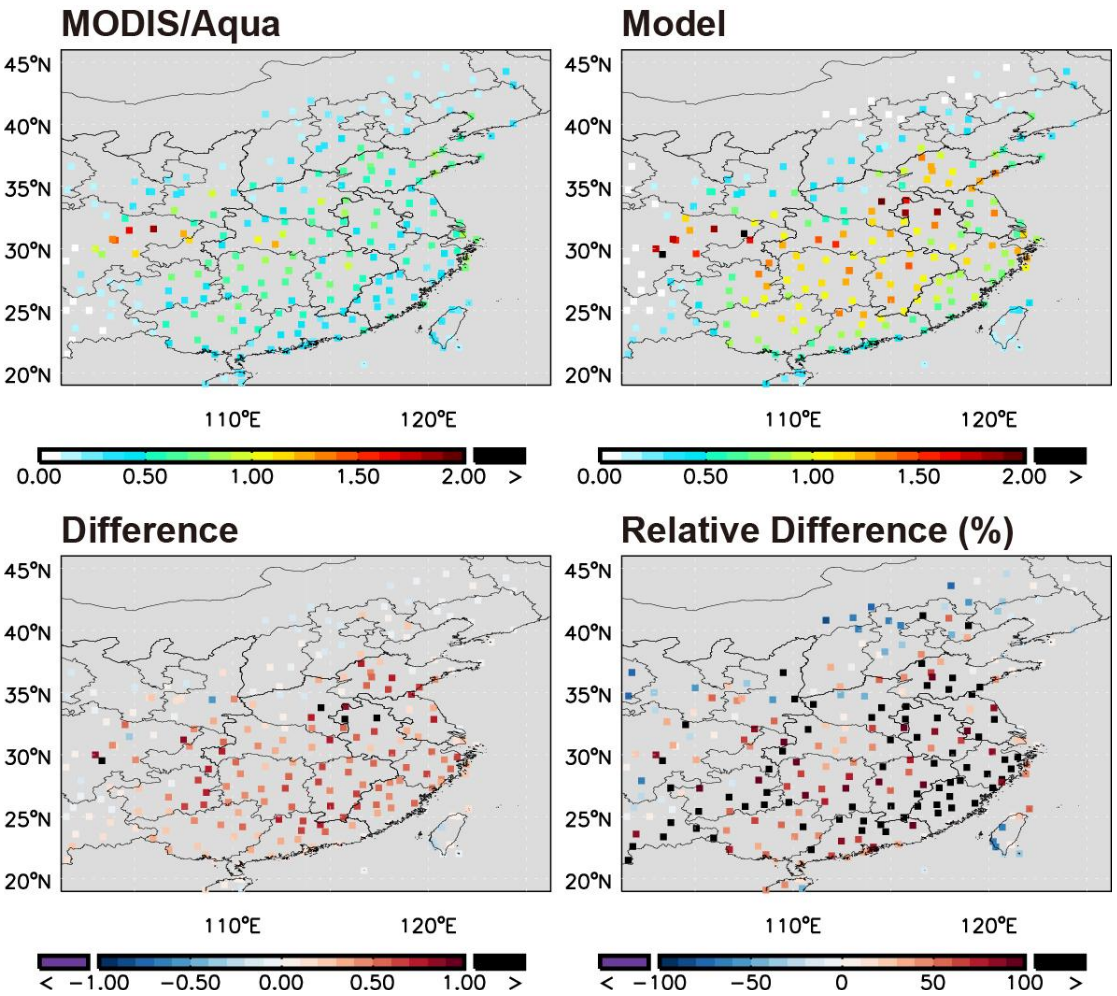

Fig. S15. Similar to Fig. S14 but for January 2006.

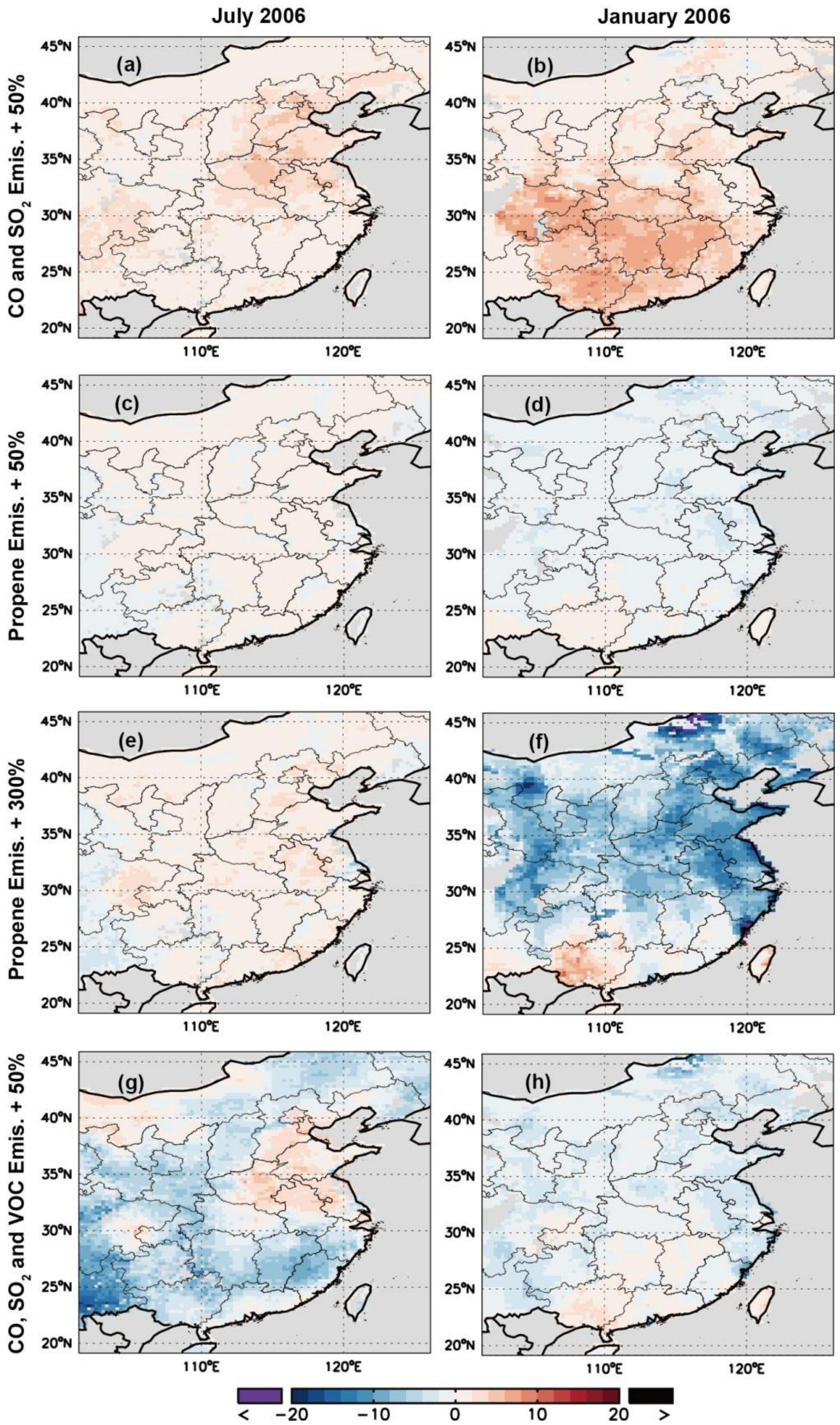

Fig. S16. Spatial distribution of percentage differences between modeled NO_2 columns with and without adjustments in emissions. (a,b) Emissions of CO and SO_2 are increased by 50%. (c,d) Emissions of propene are increased by 50%. (e,f) Emissions of propene are increased by 300%. (g,h) Emissions of CO, SO_2 and VOC are increased by 50%. Panels (e,f) are the same as Fig. 12.

References:

Carr, S., Heard, D. E., and Blitz, M. A.: Comment on "Atmospheric Hydroxyl Radical Production from Electronically Excited NO(2) and H(2)O", Science, 324, doi: 10.1126/science.1166669, 2009.

Fortems-Cheiney, A., Chevallier, F., Pison, I., Bousquet, P., Szopa, S., Deeter, M. N., and Clerbaux, C.: Ten years of CO emissions as seen from Measurements of Pollution in the Troposphere (MOPITT), Journal of Geophysical Research-Atmospheres, 116, D05304, doi: 10.1029/2010jd014416, 2011.

Global Modeling and Assimilation Office: File Specification for GEOS-5 DAS Gridded Output Document No. GMAO-1001v6.1, 2006.

Karl, T., Harley, P., Emmons, L., Thornton, B., Guenther, A., Basu, C., Turnipseed, A., and Jardine, K.: Efficient Atmospheric Cleansing of Oxidized Organic Trace Gases by Vegetation, Science, 330, 816-819, doi: 10.1126/science.1192534, 2010.

Li, S., Matthews, J., and Sinha, A.: Atmospheric hydroxyl radical production from electronically excited NO(2) and H(2)O, Science, 319, 1657-1660, doi: 10.1126/science.1151443, 2008.

Li, S., Matthews, J., and Sinha, A.: Response to Comment on "Atmospheric Hydroxyl Radical Production from Electronically Excited NO(2) and H(2)O", Science, 324, doi: 10.1126/science.1166877, 2009.

Liu, H., Crawford, J. H., Considine, D. B., Platnick, S., Norris, P. M., Duncan, B. N., Pierce, R. B., Gao, C., and Yantosca, R. M.: Sensitivity of photolysis frequencies and key tropospheric oxidants in a global model to cloud vertical distributions and optical properties, Journal of Geophysical Research, 114, D10305 (10317 pp.)-D10305 (10317 pp.)D10305 (10317 pp.), doi: 10.1029/2008jd011503, 2009.

Liu, S., and Liang, X.-Z.: Observed Diurnal Cycle Climatology of Planetary Boundary Layer Height, Journal of Climate, 23, 5790-5809, doi: 10.1175/2010jcli3552.1, 2010.

Lu, Z., Zhang, Q., and Streets, D. G.: Sulfur dioxide and primary carbonaceous aerosol emissions in China and India, 1996-2010, Atmospheric Chemistry and Physics, 11, 9839-9864, doi: 10.5194/acp-11-9839-2011, 2011.

Sander, S. P., Abbatt, J. P. D., Barker, J. R., Burkholder, J. B., Friedl, R. R., Golden, D. M., Huie, R. E., Kolb, C. E., Kurylo, M. J., Moortgat, G. K., Orkin, V. L., and Wine, P. H.: Chemical Kinetics and Photochemical Data for Use in Atmospheric Studies, Pasadena, JPL Publication 10-06, 2011.

Su, H., Cheng, Y. F., Oswald, R., Behrendt, T., Trebs, I., Meixner, F. X., Andreae, M. O., Cheng, P., Zhang, Y., and Poschl, U.: Soil Nitrite as a Source of Atmospheric HONO and OH Radicals, Science, 333, 1616-1618, doi: 10.1126/science.1207687, 2011.